NUMERICAL ANALYSIS OF THE EFFECTS OF A WIND TURBINE'S ROTATING BLADES ON THE AERODYNAMIC FORCES ON THE TOWER

Takaaki Kono[+1], Satoshi Nebucho[+2], Tetsuya Kogaki[+3],
Takahiro Kiwata[+4], Shigeo Kimura[+5], and Nobuyoshi Komatsu[+6]
[+1,2,4,5,6]Kanazawa University, Kanazawa, 920-1192 JAPAN
[+2] National Institute of Advanced Industrial Science and Technology, Koriyama, 963-0298 Japan

This study investigated the effects of the rotating blades of an upwind-type horizontal-axis wind turbine on the aerodynamic forces of the wind-turbine's tower by conducting computational fluid dynamics (CFD) simulations of the flow around the wind turbine and its tower. The CFD results confirmed that at each height above the lowest point of the rotor, the maximum value of the pressure around the tower shifted in the direction of the rotor rotation; this was caused by the diversion of air flow approaching the tower due to rotation of the blades. It was also confirmed that while a blade was passing upstream of the tower, the pressure fluctuations around the tower at each height above the lowest point of the rotor were greater on the side of the tower where the blade approaches than on the side where the blade moves away, due to the recovery of low pressure on the downstream side of the blade. In addition, it was found out that while a blade was near the tower, the air pressure on the upwind side of the tower was reduced due to interference with the lower-pressure region on the downstream side of the blade. This interference caused a periodic decrease in the drag coefficient of the tower. Moreover, it was recognized that while a blade approached the tower and then moved away, the low-pressure region on the downwind side of the blade caused a drop in the pressure on the side of the tower adjacent to the blade. This pressure drop caused a periodic fluctuation in the side force coefficient of the tower.

   Keyword: Horizontal axis wind turbine, CFD, Tower, Aerodynamic force, Blade

1. INTRODUCTION

   Accidents due to strong winds or turbulence have resulted in damage and even complete failure of wind turbines (WT) and their towers in recent years. To reduce the occurrence of incidents involving wind turbines, it is essential to design rotors and towers with the proper fatigue strength and shapes by taking into account the vibration characteristics of the tower. However, very few studies have investigated the influence of rotating blades on the aerodynamic forces on towers[1,2] and the influence of those forces on tower vibrations, so many aspects of tower behavior remain unclear at this time.

   In this study, we investigate the effects of the rotating blades of an upwind-type horizontal-axis wind turbine (HAWT) on the aerodynamic forces of the wind-turbine's tower by conducting computational fluid dynamics (CFD) simulations of the flow around the wind turbine and its tower.

2. NUMERICAL APPROACH
(1) Wind turbine and tower

   This analysis was performed on a model of the upwind HAWT used by Krogstad and Eriksen[3] in wind tunnel experiments. The diameter of the rotational area of the HAWT was $D = 894$ mm and it had 3 blades based on the NREL S826 airfoil[4] (Fig. 1). The tower had a uniform diameter in the vertical direction, $d = 61$ mm, and was divided into 5 segments of identical length, $h = 154.4$ mm, to analyze the aerodynamic forces on each segment.

[+1]t-kono@se.kanazawa-u.ac.jp, [+2]nebuchou@ryuko.ms.t.kanazawa-u.ac.jp, [+3]kogaki.t@asit.go.jp, [+4]kiwata@se.kanazawa-u.ac.jp,
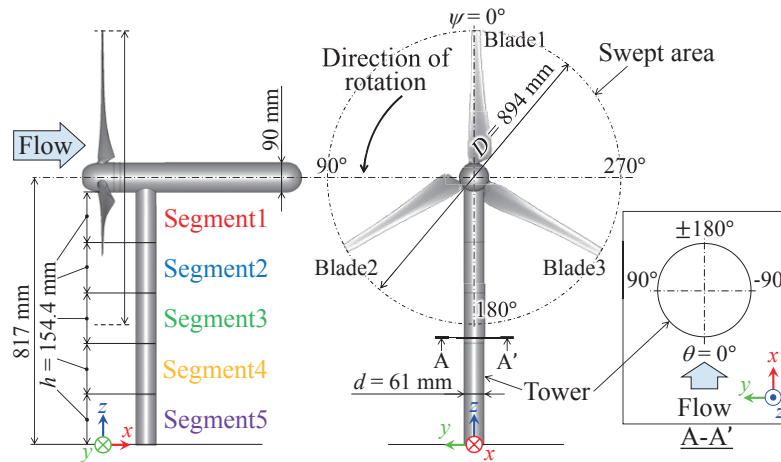[+5]skimura@se.kanazawa-u.ac.jp, [+6]komatsu@se.kanazawa-u.ac.jp

Figure 1: Outline of the wind turbine.

(2) Governing equations and discretization scheme

The CFD package ANSYS Fluent ver. 16.1 was employed. An unsteady incompressible viscous three-dimensional flow field consisting of air at 15 °C was assumed. The governing equations were the Reynolds-averaged continuity equation and Navier-Stokes equations, and were discretized by the finite volume method. The QUICK scheme was used for the advection terms, and the other terms were estimated by the second-order central difference scheme. The Reynolds stresses were computed using the k-ω shear-stress transport (SST) turbulence model[5]. The time integration was performed by a second-order implicit method. The pressure-based coupled algorithm was used to handle the coupling between pressure and velocity.

(3) Numerical setup

Fig.2 shows the computational domain and the boundary conditions. The size of the computational domain was approximately same as the wind tunnel[4], $3D \times 12.5D \times 2D$, and consisted of the rotational domain, which included the rotor, and the non-rotating exterior domain. The origin of the coordinate system was defined as the intersection of a vertical line from the center of the rotor with the floor. The total number of cells was approximately 4.5 million. The blades, tower and wind tunnel walls were covered with boundary layer meshes. The first grid node was set at 3×10^{-5} m off the surface of the blades, and was $y+ < 5$ almost over the blades. On the inlet boundary, a stream-wise wind velocity of $U_{\text{ref}} = 10$ m/s with a turbulence intensity of $TI = 0.3\%$ was implemented. On the outlet boundary, outflow boundary condition was imposed. On the surface of the blades and tower and on the wind tunnel walls, no-slip boundary conditions were set. The sliding mesh technique was used to couple the rotational domain and stationary domain. By changing the rotational speed of the rotor ω, three tip speed ratio cases were examined, $\lambda(= D\omega/2U_{\text{ref}}) = 3$, 6 and 9.
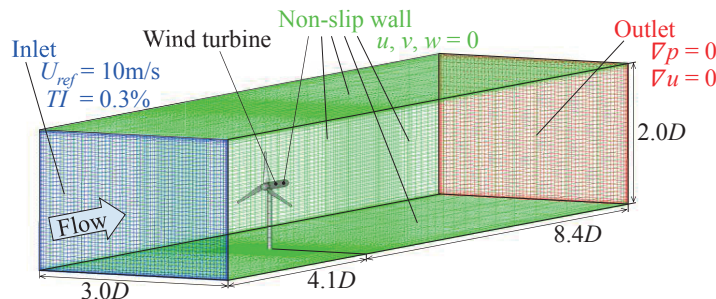

Figure 2: Computational grid and boundary conditions.

3. RESULTS AND DISCUSSION
(1) Validation of numerical approach

Fig.3 shows a comparison of the values of the power coefficient, C_P $(= 2Q\omega/\rho A U_{ref}^3)$ and thrust coefficient $C_T (= 2T/\rho A U_{ref}^2)$, evaluated from the simulations to those from the wind tunnel experiments. Here, Q is the total torque of the WT, ρ is the air density, A is the swept area and T is the total thrust of the blades. The simulations provided a reasonable qualitative and quantitative approximation of the experimentally observed results for both C_P and C_T.

Fig.4 shows comparisons between the simulation and wind tunnel experiment results of the distribution in the y direction of $\bar{u}$ at the hub height in the wind turbine wake at $x/D = 1$ at $\lambda = 6$. The calculated values for $\bar{u}$ matched the experimental results qualitatively and quantitatively well.

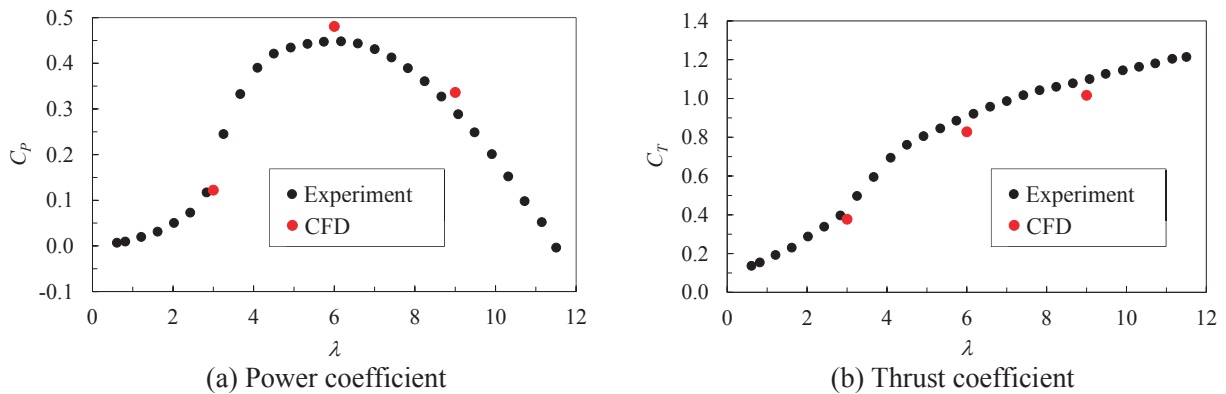(a) Power coefficient   (b) Thrust coefficient

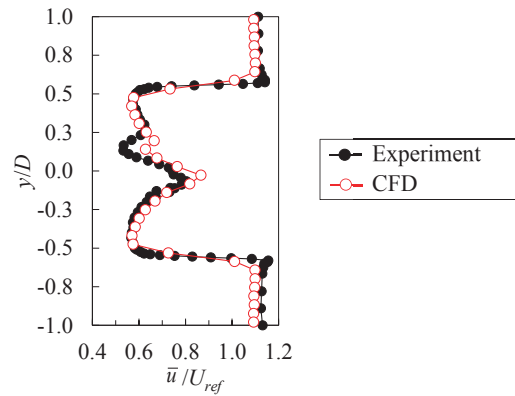Figure 3: Computational and experimental results of wind turbine performance.

Figure 4: Lateral distribution of the streamwise wind velocity at the hub height in the wind turbine wake ($x/D = 1$, $\lambda = 6$).

(2) Pressure coefficients on tower

Fig.5 presents the mean pressure coefficients C_p $(= 2(\bar{p} - \bar{p}_{ref})/ \rho U_{ref}^2)$ on the tower surface and the rms fluctuating pressure coefficients C_p' in the θ direction at the mid-heights of each tower segment at $\lambda = 6$. Here, $\bar{p}$ and $\bar{p}_{ref}$ are the time-averaged static pressure and the static pressure at the inlet boundary. C_p and C_p' show asymmetric distributions in the $\pm\theta$ directions relative to the stream-wise wind direction at segments 1–3, which are above the lowest point of the rotor. Additionally, with increasing altitude above the lowest point of the rotor, the circumferential location at which C_p reaches a maximum shifts in the $-\theta$ direction, which is the same direction as the rotor rotation. C_p' has high values in the $+\theta$ region, which is the direction from which the blade approaches. The same tendencies were observed at $\lambda = 3$ and $\lambda = 9$.
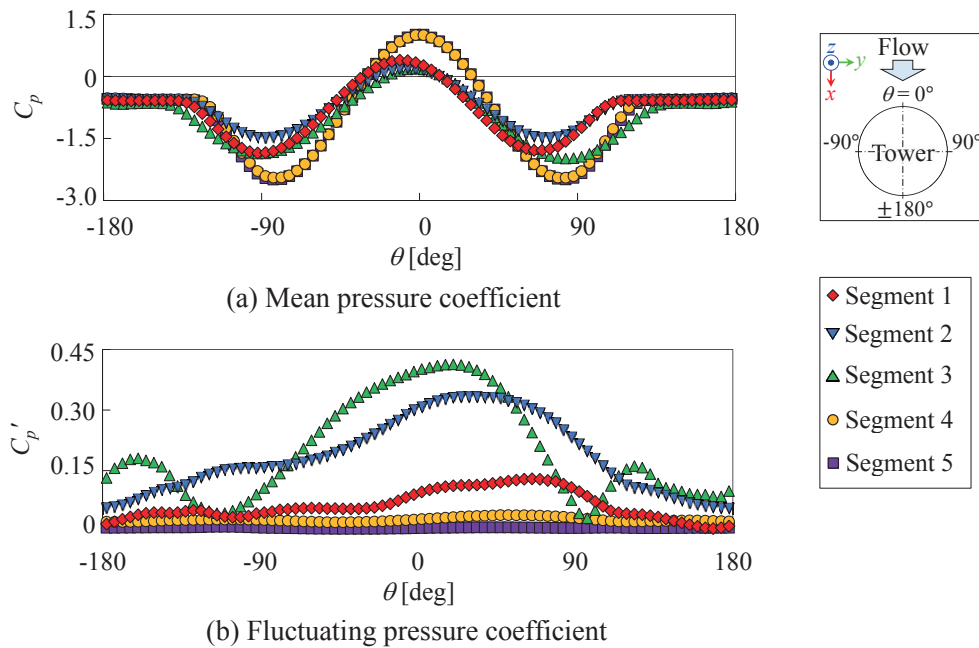
(a) Mean pressure coefficient

(b) Fluctuating pressure coefficient

Figure 5: Distributions of mean and fluctuating pressure coefficients around
the tower at the mid-heights of each segment ($\lambda = 6$).

(3) Characteristic of flow around tower

Figs.6 and 7 show the streamlines and contour plots of static pressure near the tower at the mid-height of segment 2 at $\lambda = 6$. These figures suggest the causes for the asymmetric distributions of C_p and C_p' in the $\pm\theta$ directions. The rotor azimuth ψ is defined as 0° when rotor blade #1 is pointing straight up, parallel to the tower. The positive values follow a counterclockwise direction. Thus, the chords of blades 1, 2 and 3 lie directly upwind of the tower at $\psi = 60°$, 180° and 300°. As can be seen in Fig. 6, the flows in the vicinity of the tower are diverted at all ψ. However, no such diversion is seen at segments 4 and 5. Thus, the shift of the maximum value for C_p in the $+\theta$ direction at segments 1–3 seen in Fig. 5 appears to be caused by a shift in the stagnation point, which is caused by turning of the flow toward the tower as the rotor rotates; this situation occurs at altitudes above the lowest point of the rotor. In Fig. 7, the low-pressure regions formed on the downwind side of the blade recover as the blade approaches the tower, but the pressures drop again as the blade passes and moves away from the tower. The pressure on the downwind side of the blade is clearly lower at $\psi = 50°$ than at $\psi = 70°$. The pressure at the surface of the tower interferes with the lower-pressure region on the downwind side of the blade on the $+\theta$ side than on the $-\theta$ side, and the C_p' in Fig. 5 is higher on the $+\theta$ side of the tower.
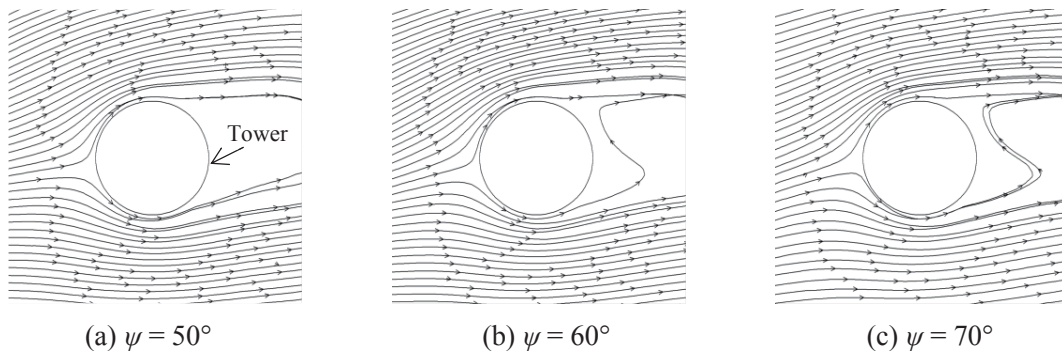

(a) $\psi = 50°$ (b) $\psi = 60°$ (c) $\psi = 70°$

Figure 6: Streamlines near the tower at the mid-height of segment 2 ($\lambda = 6$).

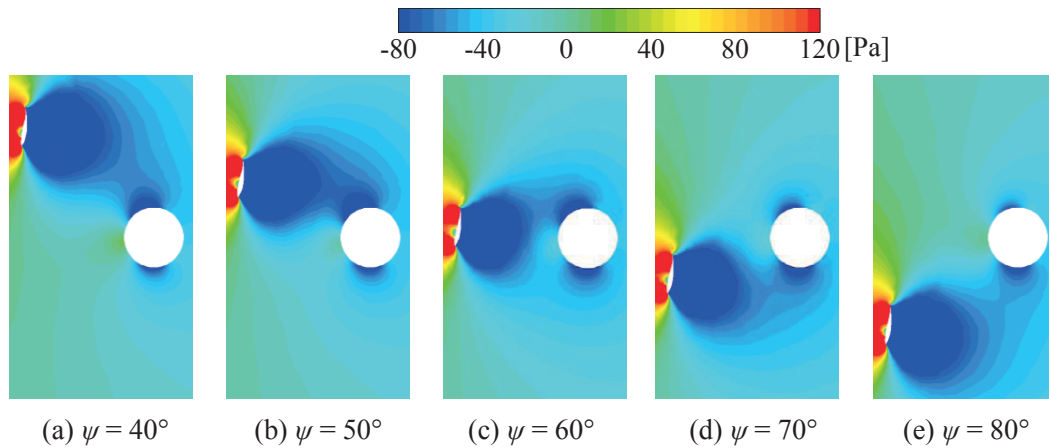(a) $\psi = 40°$　　(b) $\psi = 50°$　　(c) $\psi = 60°$　　(d) $\psi = 70°$　　(e) $\psi = 80°$

Figure 7: Contour plots of static pressure near the tower at the mid-height of segment 2 ($\lambda = 6$).

(4) Drag and lift coefficients of tower

　　Fig.8 shows the time histories of the drag coefficient C_{Fx} (= $2F_x/\rho dhU_{ref}^2$) and the lift coefficient C_{Fy} (= $2F_y/\rho dhU_{ref}^2$) on each segment of the tower at $\lambda = 6$. Here, F_x and F_y are the drag force and the lift force, respectively. The values for C_{Fx} and C_{Fy} fluctuate periodically at time intervals corresponding to when the blade passes upwind of the tower. Segments 1–3, which are affected by the passing of the blades upstream, show particularly high amplitudes of fluctuation. One reason C_{Fx} drops as a blade approaches the tower is the interference from the low-pressure region downwind of the blade, and the resulting drop in air pressure on the upwind side of the tower, as shown in Fig. 7. As also shown in Fig. 7, the reason for the periodic fluctuation in C_{Fy} is the low-pressure region downwind of the blade lowers the pressure on the $+\theta$ side and then on the $-\theta$ side of the tower as the blade approaches and then moves away from the tower.
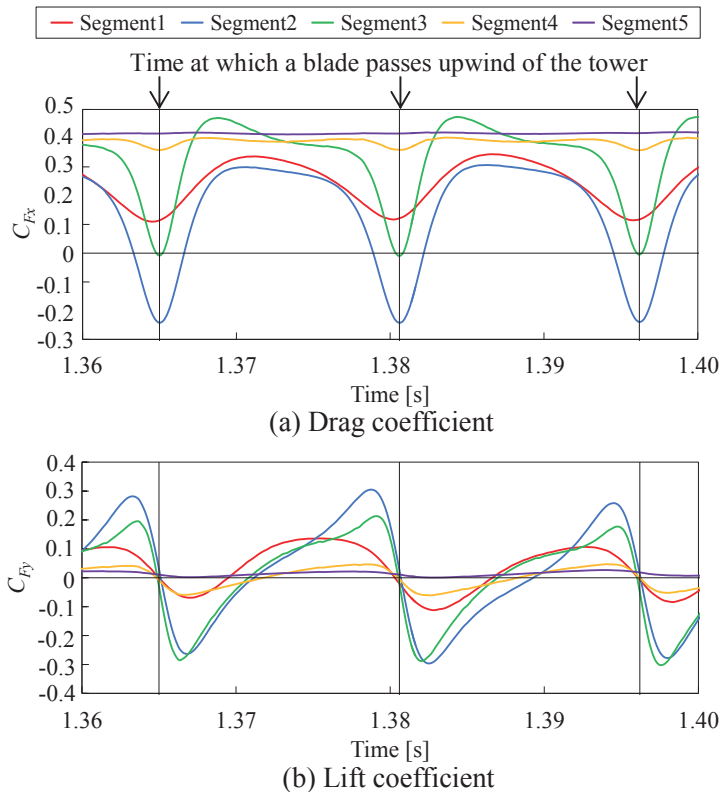

(a) Drag coefficient

(b) Lift coefficient

Figure 8: Time-history of the aerodynamic force coefficients on each segment of the tower ($\lambda = 6$).

4. CONCLUSIONS

The influence of rotating wind turbine blades on the aerodynamic characteristics of a wind turbine tower was examined by conducting computational fluid dynamics analysis and the following findings were obtained.

(1) As a result of the diversion of air flow approaching the tower due to rotation of the blades, the maximum value of pressure around the tower at each height above the lowest point of the rotor shifts in the direction of the rotor rotation.

(2) While a blade is passing upstream of the tower, the pressure fluctuations around the tower at each height above the lowest point of the rotor are greater on the side of the tower where the blade approaches than on the side where the blade moves away, due to the recovery of low pressure on the downstream side of the blade.

(3) While a blade is near the tower, the air pressure on the upwind side of the tower is reduced due to interference with the lower-pressure region on the downstream side of the blade. This interference causes a periodic decrease in the drag coefficient of the tower.

(4) While a blade approaches the tower and then moves away, the low-pressure region on the downwind side of the blade causes a drop in the pressure on the side of the tower adjacent to the blade. This pressure drop causes a periodic fluctuation in the lift coefficient of the tower.

REFERENCES

1) Gomez-Iradi, S., Steijl, R., Barakos, G. N.: Development and validation of a CFD technique for the aerodynamic analysis of HAWT, *Journal of Solar Energy Engineering*, Vol. 131, 031009.1-031009.13, 2009.

2) Wang, Q., Zhou, H., Wan, D.: Numerical simulation of wind turbine blade-tower interaction, *Journal of Marine Science and Application*, Vol. 11, pp. 321-327, 2012.

3) Krogstad, P.-Å., Eriksen, P.E., "Blind test" calculations of the performance and wake development for a model wind turbine, *Renewable Energy*, Vol. 50, pp. 325-333, 2013.

4) Somers, D.M.: The S825 and S826 Airfoils," National Renewable Energy Laboratory, NREL/SR-500-36344, 2005.

5) Menter, F. R., Langtry, R. B., Likki, S. R., Suzen,Y. B., Huang, P. G., Volker, S.: A correlation-based transition model using local variables—Part I:Modelformu-lation. *Journal of Turbomachinery*, Vol. 128, pp. 413-422, 2006.